RSC Advances

PAPER

Cite this: *RSC Adv.*, 2022, **12**, 13557

Effects of organic components in cuttlebone on the morphological and mechanical properties of peroxide cross-linked cuttlebone/natural rubber composites†

Thitipat Chongcharoenchaikul,[abc] Kosuke Miyaji,[ac] Preeyanuch Junkong,[cd] Sirilux Poompradub *[bcef] and Yuko Ikeda *[cg]

The clarification of the role of organic components in cuttlebone particles on the morphological and mechanical properties in terms of the strain-induced crystallization (SIC) of peroxide cross-linked cuttlebone/natural rubber (NR) composites was revealed for the first time in this study. The organic components in cuttlebone particles affected the increased bound rubber layers and the decreased rubber chain orientation due to the formation of interfacial interactions (filler-to-filler and/or filler-to-rubber interactions). During SIC, the presence of organic components in cuttlebone particles did not significantly affect the crystallinity index and crystallite size in cuttlebone/NR composites. The increased moduli in the stress–strain curve resulted from the presence of biofiller, SIC, and organic components in the cuttlebone. Therefore, the presence of organic components in biofiller is an important factor in improving the mechanical properties of green rubber composite materials.

Received 23rd March 2022
Accepted 15th April 2022

DOI: 10.1039/d2ra01885c

rsc.li/rsc-advances

Introduction

The development of green materials from biorenewable resources has become of great concern as a means to decrease the problems of global warming and resource scarcity. Natural rubber (NR) is an essential sustainable elastomer that has been widely used in the different rubber industries for several decades due to its outstanding properties, based on its elasticity, that cannot be easily mimicked by synthetic rubber or polymer elastomers.[1–7] In terms of sustainable development, the reinforcing fillers from renewable resources have attracted the attention of many researchers for solving environmental problems, including the use of bamboo,[8–13] wood pulp,[14–16] and leaves.[17–20]

Most biofillers are derived from agricultural feedstocks and contain only organic components. However, animal bones are also renewable feedstocks that can be used as a filler. Biofillers from animal bones are different from agricultural feedstocks in that they contain a marked amount of both inorganic and organic components. Several studies have investigated the possibility of marine wastes, such as cuttlebone,[21–26] seashells,[27] or chitin,[28–31] as a reinforcing filler in polymer composite materials. Cuttlebone, which is obtained from marine waste, is one such bio-reinforcing filler that has been shown to have an effective reinforcement effect in various kinds of polymers, such as epoxy resin,[24,25] polyurethane,[26] or NR.[22,23] Cuttlebone consists of inorganic calcium carbonate ($CaCO_3$) compounds and organic compounds of proteins and chitins.[22,23,32] A few studies have confirmed that the reinforcing effect of cuttlebone in NR composites was achieved by the presence of organic compounds in cuttlebone.[22,23] The use of cuttlebone as a biofiller in NR composites did not prevent the vulcanization of NR in both peroxide and sulfur cross-linking processes.[22,23] Moreover, the organic compounds in cuttlebone showed a synergistic effect that enhanced the compatibility and mechanical properties of NR composites with non-rubber components in NR.[33]

The strain-induced crystallization (SIC) behavior is an indispensable behavior that explains the mechanical properties of a composite material based on the structural changes during stretching.[6,34] Various factors that affect the SIC behavior of

[a]*Graduate School of Science and Technology, Kyoto Institute of Technology, Matsugasaki, Sakyo, Kyoto 606-8585, Japan*
[b]*Department of Chemical Technology, Faculty of Science, Chulalongkorn University, Phatumwan, Bangkok 10330, Thailand. E-mail: sirilux.p@chula.ac.th*
[c]*Center for Rubber Science and Technology, Kyoto Institute of Technology, Matsugasaki, Sakyo, Kyoto 606-8585, Japan. E-mail: yuko@kit.ac.jp*
[d]*Department of Chemistry, Faculty of Science, Mahidol University, Ratchathewee, Bangkok 10400, Thailand*
[e]*Center of Excellence on Petrochemical and Materials Technology, Chulalongkorn University, Phatumwan, Bangkok 10330, Thailand*
[f]*Green Materials for Industrial Application Research Unit, Faculty of Science, Chulalongkorn University, Phatumwan, Bangkok 10330, Thailand*
[g]*Faculty of Molecular Chemistry and Engineering, Kyoto Institute of Technology, Matsugasaki, Sakyo, Kyoto 606-8585, Japan*

† Electronic supplementary information (ESI) available. See https://doi.org/10.1039/d2ra01885c

rubber composite materials have been reported, such as the network-chain density,[35–40] rubber type,[36,41–48] vulcanizing system,[49] and filler type.[50–55] Many studies have also investigated the effects of commercial reinforcing fillers, such as carbon black,[50–55] $CaCO_3$,[50] or silica,[51–53] on the SIC of polymer composites. To date, there have been few reports on the investigation of the SIC behavior of NR composites using lignin as a biofiller.[56,57] The effect of cuttlebone as the biofiller, including both inorganic and organic components on the SIC in both NR and synthetic rubber composites using the sulfur cross-linking system, was also investigated in the previous article.[33] However, there is no report on the SIC of peroxide cross-linked cuttlebone/NR composites.

Accordingly, this study has focused on the synergistic effects of the cuttlebone particles on the morphology and mechanical behavior in terms of the SIC of peroxide cross-linked NR composites. Natural cuttlebone particles with organic components (CTBO) and the derived cuttlebone particles without organic components (CTB) were prepared. Atomic force microscopy (AFM) was performed to demonstrate the surface properties of cuttlebone/NR composites and the compatibility between cuttlebone particles and NR matrices. The network-chain densities and bound rubber content were estimated to support the morphological results. The mechanical properties and SIC phenomenon of cuttlebone/NR composites were examined by the simultaneous synchrotron time-resolved wide-angle X-ray diffraction (WAXD)/tensile measurements. Finally, the SIC mechanism of peroxide cross-linked cuttlebone/NR composites was proposed.

Experimental section

Materials

Standard Thai rubber 5L (STR-5L) was obtained from the PI Industry Ltd (Thailand). Dicumyl peroxide (DCP, PERCUMYL D, Nichiyu Co. Ltd) was used as a curing agent. The CTBO particles (93 wt% of $CaCO_3$ and 7 wt% of organic components) were obtained from waste stocks at Siam Ocean Food Co., Ltd (Thailand), crushed and sieved to pass through a 37 μm-mesh sieve. The CTB particles (100 wt% of $CaCO_3$) were prepared by calcination of the CTBO particles at 400 °C for 30 min. Both CTBO and CTB particles (with average particles size of 29 and 23 μm) were dried at 120 °C for 2 h before use.

Preparation of peroxide cross-linked cuttlebone/NR composites

In order to observe the effects of organic components in cuttlebone particles on morphological and mechanical properties, the CTBO or CTB particles were used at 50 parts per hundred of rubber (phr) with 2 phr DCP as a curing agent. Both components were mixed with NR by a two-roll mill at room temperature to prepare the rubber compounds. The compounds were then heat-pressed at 155 °C and 150 kg m^{-2} for 30 min to obtain a 1 mm thick rubber sheet. The samples were coded as NRCTBO, NRCTB and NRP for the CTBO/NR composite, CTB/NR composite and peroxide cross-linked unfilled NR, respectively.

Morphological analysis

The morphology of the peroxide cross-linked cuttlebone/NR composites was determined by AFM using a SEIKO SPA-400 (Seiko Instruments Inc., Japan). The sample was prepared to a 10 mm × 10 mm × 1 mm sheet by knife at ambient temperature (25 °C) and then subjected to AFM in the dynamic force microscope (DFM) mode with a scan speed of 0.3 Hz and a scan area of 100 μm × 100 μm under ambient conditions. The cantilever was the Micromasch HQXSC11 type B with a resonance frequency of 84.48 kHz, force constant of 3.15 N m^{-1} and sensitivity of 31.99 nm V^{-1}. Gwyddion software was used to evaluate the quantitative analysis in terms of roughness (R_a).

Determination of network-chain densities

The modified Flory–Rehner equation was used to estimate the network-chain densities (υ) of the peroxide cross-linked NR composites based on the swelling test in toluene at 25 °C for 48 h as follows:[42,58]

$$\upsilon = -\frac{1}{V}\left[\frac{\ln(1-V_r)+V_r+\chi V_r^{2}}{g^{2/3}V_r^{1/3}-\frac{V_r}{2}}\right] \quad (1)$$

$$V_r = \frac{\left(\frac{W_{ini}}{\rho_{rubber}}-\frac{W_{ini}\times f_{filler}}{\rho_{filler}}\right)}{\left(\frac{W_{ini}}{\rho_{rubber}}-\frac{W_{ini}\times f_{filler}}{\rho_{filler}}\right)+\left(\frac{W_{fin}-W_{ini}}{\rho_{solvent}}\right)} \quad (2)$$

$$g = \frac{W_d}{W_{ini}} \quad (3)$$

where V is the molar volume of the solvent (106.3 cm^3 mol^{-1} for toluene), V_r is the volume fraction of the rubber in the swollen state, χ is the rubber–solvent interaction parameter (Flory–Huggins parameter), which was assumed as 0.39 for NR/toluene,[42] g is the gel fraction, W_{ini} is the initial weight of the sample before swelling, W_{fin} is the weight of the sample after being swollen for 48 h, W_d is the weight of the dry sample after swelling, f_{filler} is the weight fraction of filler in the un-swollen state, and ρ_{rubber}, ρ_{filler} and $\rho_{solvent}$ are the densities of the rubber, filler and solvent, respectively.

Determination of bound rubber content

The bound rubber content (BRC) was measured by soaking 1 g of uncross-linked NR filled with 50 phr CTB or CTBO particles in toluene for 7 days at the ambient temperature. The extracted rubber was dried at 60 °C for 24 h and weighed. The BRC was calculated from eqn (4);[58]

$$\text{Bound rubber content } (\%) = \frac{W_1-(W_0\times M_f)}{(W_0\times M_r)}\times 100 \quad (4)$$

where W_1 is the weight of the dried sample after extraction, W_0 is the initial weight of the sample, M_f is the weight fraction of filler in the sample and M_r is the weight fraction of rubber in the sample.

Simultaneous tensile and synchrotron time-resolved WAXD measurements and WAXD analysis

Simultaneous WAXD and tensile measurements were performed using a synchrotron radiation system at the BL-40XU beamline of SPring-8 in Harima, Japan.[59] A custom-made tensile tester (ISUT-2201, Aiesu Giken Co., Kyoto, Japan) was situated on the beamline, and WAXD patterns were recorded during the tensile measurement at ambient temperature according to the previous experiments.[38,45,53] The wavelength of the X-rays was 0.0832 nm and the camera length was 118 mm. Two-dimensional (2D) WAXD patterns were recorded using a charge-coupled device (CCD) camera (ORCA II, Hamamatsu Photonics Co., Japan). The intensity of the incident X-rays was attenuated using an aluminum plate equipped on the beamline and the incident beam was exposed to the sample for 70 ms every 3 s. A ring-shaped sample with the external and internal diameters of 13.7 and 11.7 mm, respectively, was subjected to the tensile measurements in order to correctly determine the stretching ratio (α) of the deformed sample, which was calculated from the ratio of the extended length to the initial length. The stretching speed was 100 mm min^{-1}. During deformation, the sample dimensions were changed in both the transverse and longitude directions. Therefore, the Poisson's ratio was measured separately under the similar experimental conditions of simultaneous WAXD and tensile measurements using a CCD camera (VC1000 Digital Fine Scope, OMRON Co., Japan).[53]

The obtained 2D-WAXD images were analyzed using the "POLAR" software (Stonybrook Technology & Applied Research, Inc.). The three structural parameters of "crystallinity index (CI)", "oriented amorphous index (OAI)" and "oriented index (OI)" of each stretched sample were evaluated. These structural parameters were azimuthally integrated within the range of $\pm 75^\circ$ from the equator and defined by eqn (5)–(7):[38,45,53]

$$\mathrm{CI} = \frac{\sum_{\text{crystal}} 2\pi \int \sin\phi \mathrm{d}\phi \int I(s)s^2 \mathrm{d}s}{\sum_{\text{total}} 2\pi \int \sin\phi \mathrm{d}\phi \int I(s)s^2 \mathrm{d}s} \quad (5)$$

$$\mathrm{OAI} = \frac{\sum_{\text{oriented amorphous}} 2\pi \int \sin\phi \mathrm{d}\phi \int I(s)s^2 \mathrm{d}s}{\sum_{total} 2\pi \int \sin\phi \mathrm{d}\phi \int I(s)s^2 \mathrm{d}s} \quad (6)$$

OI was obtained by the summation of CI and OAI as in eqn (7):

$$\mathrm{OI} = \mathrm{CI} + \mathrm{OAI} \quad (7)$$

where $I(s)$ represents the intensity distribution of each peak obtained from the WAXD pattern, s is the radial coordinate in reciprocal space (nm^{-1}), estimated from $s = 2(\sin\theta/\lambda)$, where λ is the wavelength and 2θ is the scattering angle, and ϕ is the angle between the scattering vector of the peak and the fiber direction. For the structural parameter calculation, the air scattering, the isotropic amorphous scattering and the cuttlebone particle's crystalline reflection were subtracted from the WAXD patterns of each sample to leave only the oriented amorphous scattering and crystalline reflections of NR (Fig. S1†). The peak fitting for the crystal planes of 200, 201, 120, and 121 leads to the numerators based on eqn (5) and (6). The remaining broad peaks were then ascribed to oriented amorphous segments.

The apparent crystallite sizes were estimated by using the Scherrer equation (eqn (8)):[50]

$$L_{hkl} = K\lambda/(\beta \cos\theta) \quad (8)$$

where L_{hkl} is the apparent crystallite size in the direction perpendicular to the (hkl) plane and θ is the Bragg angle (half of the scattering angle). A K value of 0.89 was used in this study.[45]

Results and discussion

Morphology of peroxide cross-linked cuttlebone/NR composites

Fig. 1 shows the AFM images in terms of the height and phase of NRP, NRCTBO and NRCTB. The height image of NRP in Fig. 1(a) shows a smooth surface with R_a of 34.03 nm. The presence of CTBO or CTB particles in NR matrix affected the increased R_a values of NRCTBO (112.8 nm) and NRCTB (141.2 nm), respectively. It is worth noting that the R_a value of NRCTBO was lower than that of NRCTB. This observation could be due to the good compatibility of CTBO particles with the NR matrix that might come from the presence of organic components in CTBO particles.

In the phase images (Fig. 1(b)), NRCTBO represented the harmonious colors with the foggy interface regions between CTBO particles and the NR matrix, whereas NRCTB clearly showed the phase difference around the interface regions of CTB particles in the NR matrix. Moreover, the BRC of NRCTBO was higher than that of NRCTB (Table 1). As a result, the organic components, such as protein or chitin, in the cuttlebone particles might interact with non-rubber components in the NR matrix to form the large bound rubber layer around the cuttlebone particles,[33] resulting in good compatibility between the inorganic filler ($CaCO_3$) and the NR matrix of the peroxide cross-linked NR composites.

Tensile properties and SIC of peroxide cross-linked cuttlebone/NR composites under uniaxial deformation

The good compatibility between cuttlebone particles with organic components and the NR matrix might promote the enhanced mechanical properties of NRCTBO as compared to NRCTB. To confirm this hypothesis, the tensile stress–strain curves of the NRP, NRCTBO, and NRCTB are presented in Fig. 2(a). At the same α, the stresses of both the NRCTBO and NRCTB composites were higher than that of the NRP until the rupture of each sample due to the reinforcing effect of the respective cuttlebone particles. In particular, the CTBO particles showed greater reinforcing ability than the CTB particles. The elongations at break for NRCTBO and NRCTB were shorter than that for NRP because of their higher stiffness. Moreover, NRCTBO seemed to bear higher stress than NRCTB at the same α. This difference clearly showed the effect of the organic components in the cuttlebone particles on enhancing

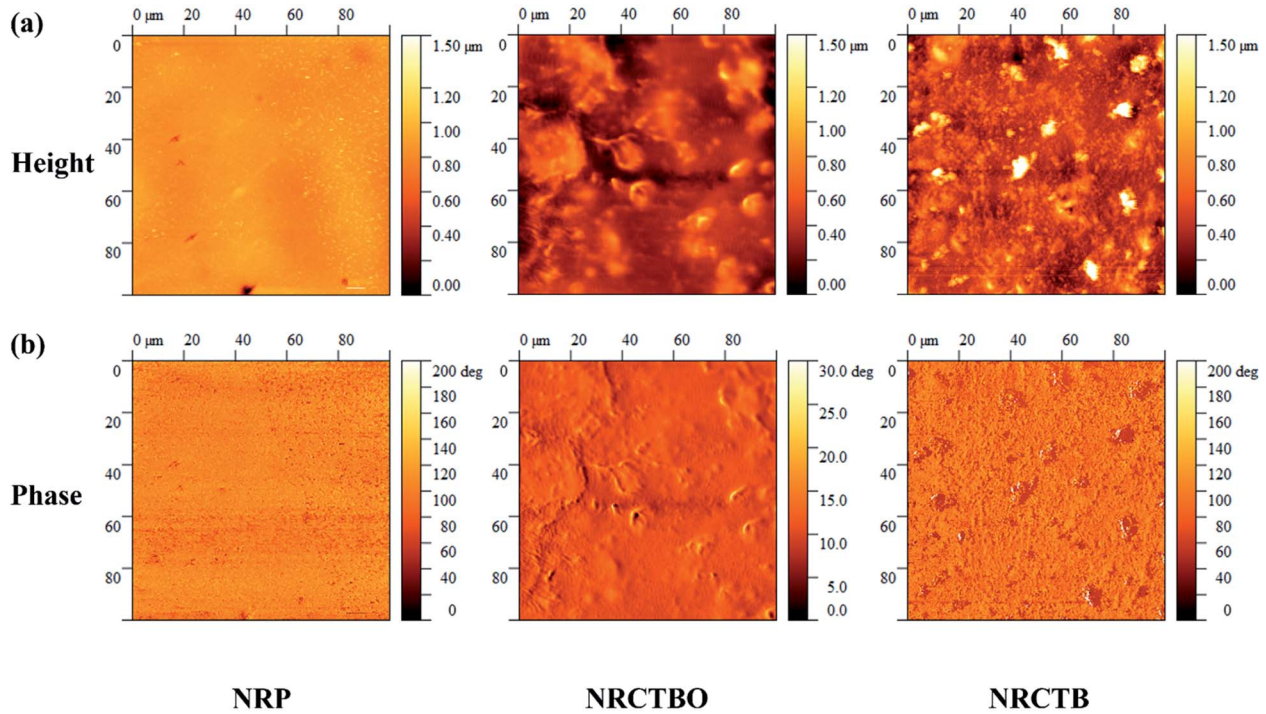

Fig. 1 AFM images in terms of (a) height and (b) phase images of the NRP, NRCTBO, NRCTB.

the reinforcement of the cuttlebone/NR composites by increasing the filler-to-rubber interactions and acting as the reinforcer with cuttlebone particles.

A significant change in the slope of the stress–strain curves was observed at $\alpha \approx 4.0$ for NRP and 3.5 for NRCTBO and NRCTB, respectively, due to the SIC. To understand the effect of the cuttlebone particles with organic components on the SIC behavior of peroxide cross-linked cuttlebone/NR composites, the tensile/WAXD measurements were firstly investigated in this study. The WAXD patterns of NRP, NRCTBO, and NRCTB during the stretching process are illustrated in Fig. 2(b–d). Before NRP deformation, an amorphous halo ring, which indicated the randomly coiled amorphous NR chains, was observed, as seen in Fig. 2(b). After the sample was stretched up to $\alpha \approx 4.0$, the NRP showed the small peaks of crystallites in the WAXD pattern. This appearance of a crystalline reflection is due to the arrangement of rubber chains as the starting site for SIC. Upon further deformation, the crystalline reflection intensities increased gradually and were observed at an α of 5.75. This behavior shows the general information for the SIC of NR.[35,38,49]

It is important to note that the $CaCO_3$ reflections were observed in the WAXD patterns of NRCTBO and NRCTB (Fig. 2(c and d)). This result is in an agreement with a previous WAXD pattern of a commercial $CaCO_3$-filled NR composite material.[50] The same SIC behavior was also observed in the case of the NRCTBO and NRCTB composites with slightly lower intensities of crystalline reflections as compared to the unfilled one. In addition, the crystallite peaks of the NRCTBO and NRCTB composites occurred at lower α as compared to the unfilled NRP. However, the crystalline reflections of rubber chains in both NR composite materials still appeared at the same positions as in the unfilled sample. Therefore, the CTBO and CTB particles used in this study disturbed the rubber chain orientation during the SIC of peroxide cross-linked NR composites.

The quantitative analysis of SIC parameters (OI, OAI, and CI) was conducted to investigate the SIC behaviors of peroxide cross-linked cuttlebone/NR composites as shown in Fig. 2(e–g). Such SIC parameters were considered based on the following assumption: the orientation occurred only in the rubbery phase whereas the fillers (CTBO and CTB) and BRC were presumed as the immobilized phases. The OI values for all samples tended to increase upon the increase in α. This is due to the increased orientation of amorphous rubber chains during the deformation. However, the addition of cuttlebone particles reduced the

Table 1 BRC, network-chain density and crystallite size in the (*hkl*) plane of the NRCTBO and NRCTB composites compared to the unfilled NRP

Sample code	BRC (%)	$\nu \times 10^{4a}$ (mol cm^{-3})	$L_{200}{}^{b}$ (nm)	$L_{120}{}^{b}$ (nm)	$L_{002}{}^{b}$ (nm)
NRP	—	1.4 ± 0.0	23.1	11.8	17.3
NRCTBO	28 ± 2	2.4 ± 0.1	19.7	10.6	15.1
NRCTB	24 ± 2	2.2 ± 0.2	18.1	10.0	15.4

[a] Network-chain density calculated by the modified Flory–Rehner equation. [b] Crystallite size was calculated by the Scherrer equation at $\alpha = 5.75$.

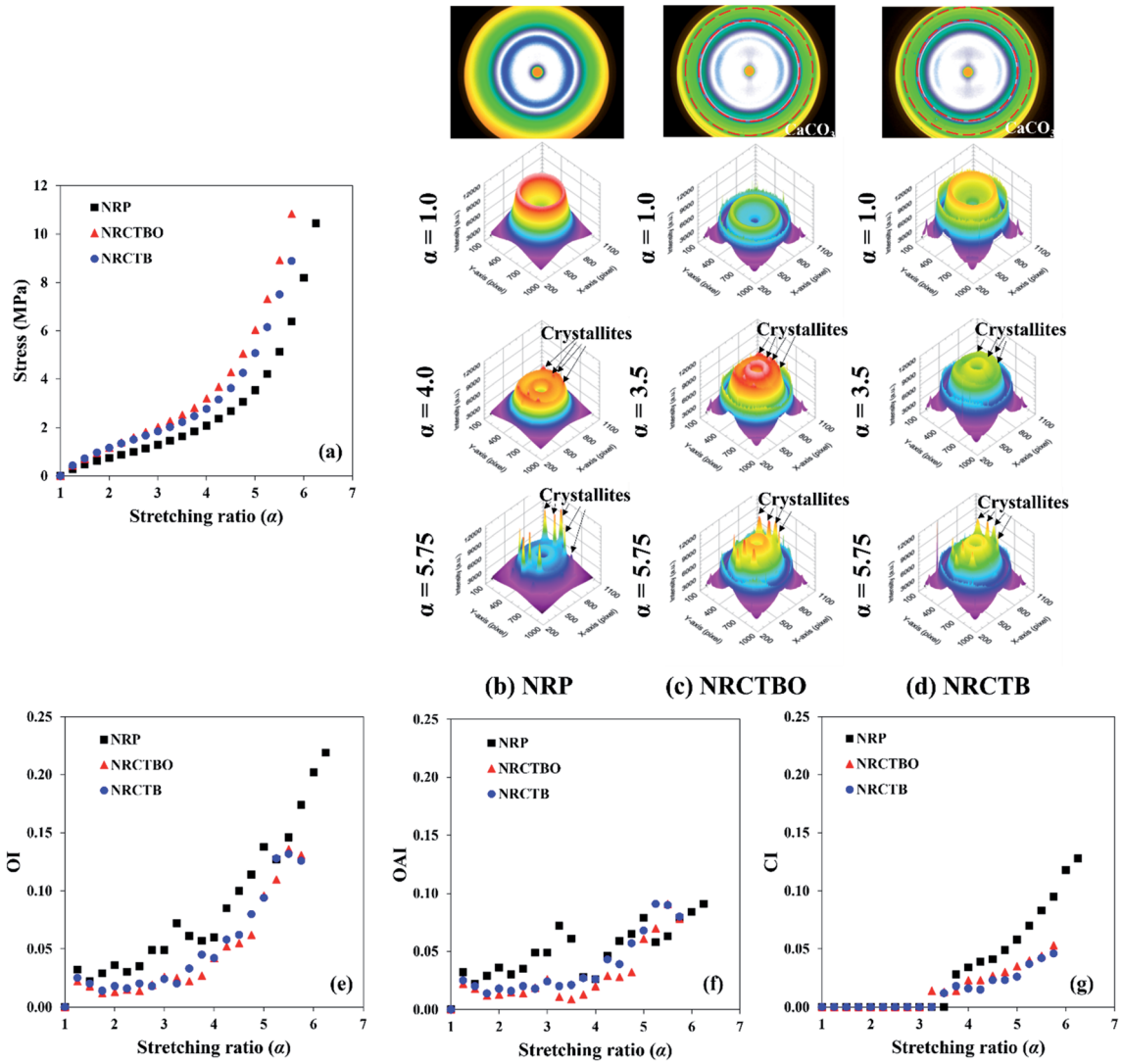

Fig. 2 (a) Stress–strain curves of the NRP, NRCTBO, and NRCTB composites against the stretching ratios under uniaxial deformation, the representative WAXD images of the (b) NRP, (c) NRCTBO, (d) NRCTB composites at different stretching ratios (α). Plots of (e) OI, (f) OAI, (g) CI of the NRP, NRCTBO, and NRCTB composites against the stretching ratios under uniaxial deformation. The red circles in (b–d) represent the $CaCO_3$ reflections of the cuttlebone particles.

OI values of both composites due to the formation of filler-to-filler and/or filler-to-rubber interactions in peroxide cross-linked cuttlebone/NR composites.

At low deformation, the OAI values of NRP seemed to fluctuate, while the OAI values of NRCTBO and NRCTB changed slowly and were found to be lower than that of NRP (Fig. 2(f)) because the cuttlebone particles might disturb the NR chain orientation. The OAI values of NRCTBO were slightly decreased when compared to NRCTB, which indicated that the high BRC (Table 1) from the organic components in CTBO particles may also decrease the NR chain orientation.

Fig. 2(g) shows the relationship between the CI values and α for all samples. Generally, the CI value was detected when the SIC crystallites operated and the first α that obtained the CI value was noted as the onset of SIC (α_c). The α_c for NRCTBO, NRCTB and NRP were at α = 3.25, 3.50 and 3.75, respectively. The slight decrease in α_c in the case of peroxide cross-linked cuttlebone/NR composites was ascribable to the differences in the network heterogeneity by the filler addition. The CI values for all samples tended to increase with increasing α. However, the increased CI rate in the NRCTBO and NRCTB composites was slower than that in NRP. The maximal CI values of NRCTBO and NRCTB were almost half the CI values of NRP because the cuttlebone particles prevented the NR chain orientation. Accordingly, the organic components in cuttlebone particles did not significantly affect the CI value during the stretching process, resulting in comparable CI values and crystallite sizes (L_{200}, L_{120}, and L_{002}) with NRCTB as shown in Table 1.

Relationship between SIC and stress of peroxide cross-linked cuttlebone/NR composites

The relationship between the SIC and tensile characteristics was investigated and the plots in terms of OI, OAI, and CI values

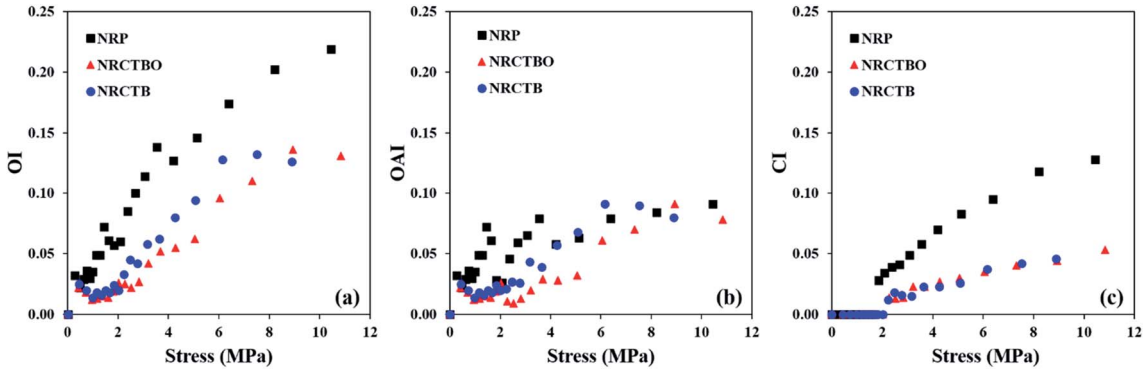

Fig. 3 Plots of (a) OI, (b) OAI and (c) CI of NRP, NRCTBO and NRCTB composites against stress.

against the stress are shown in Fig. 3. A clear difference was observed in the OI values between the unfilled and cuttlebone/NR composites (Fig. 3(a)). The decreased OI values of NRCTBO and NRCTB as compared to the unfilled sample at the same stress loading indicated that cuttlebone particles could act as a reinforcer in the NR composites.

Fig. 3(b) shows the plot between the OAI value and the stress during SIC. This relationship was focused on the oriented rubber chains that could load stress during the deformation. At low stress (<6 MPa), the OAI values of NRCTBO and NRCTB were lower than those of NRP due to the stress sharing of the rigid cuttlebone particles with the NR segments and the prevention of the NR chain orientation by cuttlebone particles. One of the interesting points is that the OAI value of NRCTBO was slightly lower than that of NRCTB, which confirmed that the presence of organic components in cuttlebone particles increased the BRC in NRCTBO (Table 1), resulting in more stress being loaded to the immobilized phases and impeding the orientation of some NR chains. However, the OAI values for all samples seemed to be comparable when the stresses were greater than 6 MPa due to the limitation of rubber chain orientation between the crosslinking points.

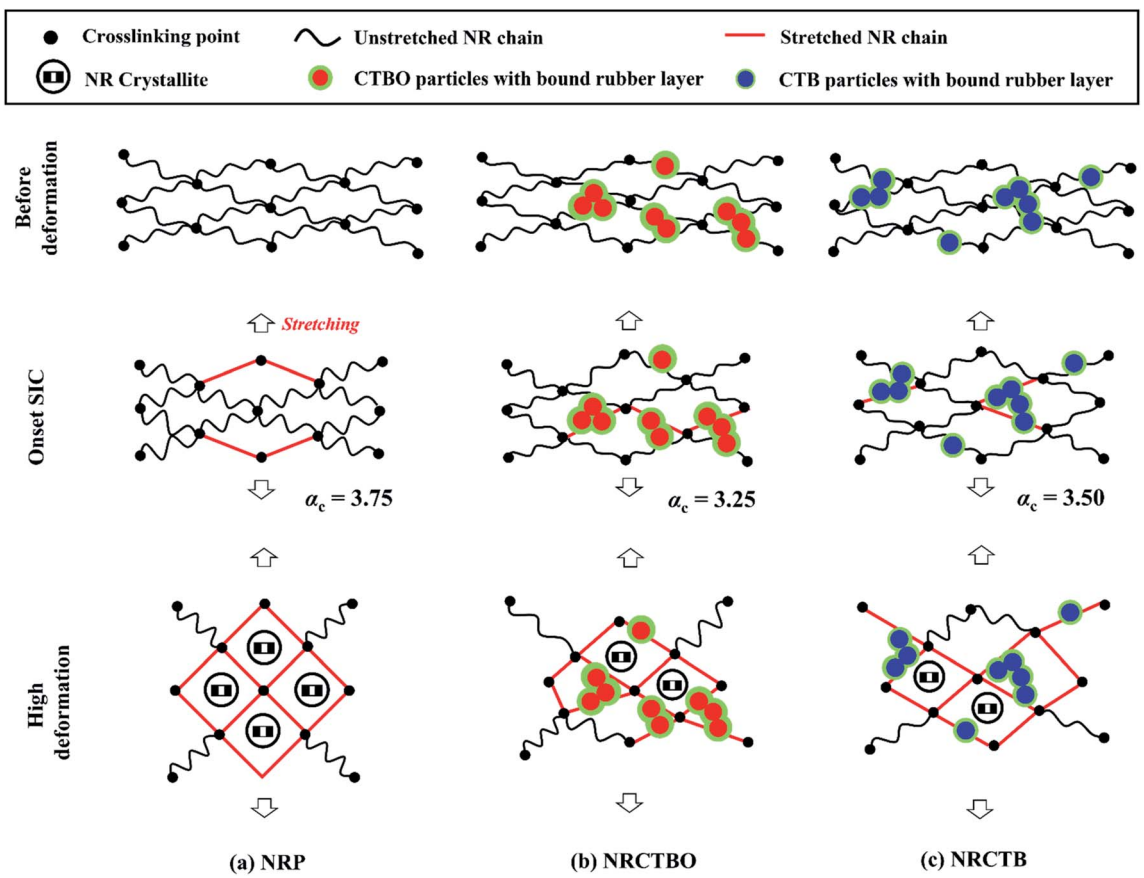

Fig. 4 Models of SIC mechanism of (a) NRP, (b) NRCTBO and (c) NRCTB.

Concerning the relationship between the CI value and the stress, as seen in Fig. 3(c), the CI value was not observed at the initial deformation until the onset SIC appeared. Thereafter, the CI value rapidly increased because the oriented amorphous segments were crystallized. The CI values of the NRCTBO and NRCTB were lower than those of NRP due to the decreased volume fraction of the rubbery matrix in cuttlebone/NR composites. This observation might indicate that the cuttlebone particles can bear the stress as a reinforcing filler together with the crystallites generated during SIC. However, the CI values of both NRCTBO and NRCTB were comparable. It was suggested that the stress loading on NR crystallites in peroxide cross-linked cuttlebone/NR composites may not be improved by the organic components in cuttlebone particles.

SIC mechanism of cuttlebone/NR composites

Accordingly, the representative model for SIC in cuttlebone with/without organic components was proposed as seen in Fig. 4. Before deformation ($\alpha = 1.0$), NRP consisted of rubber chains (black lines) and crosslinking points (black dots) from peroxide crosslinks. During deformation, some rubber chains were oriented as the stretched rubber chains (red lines) and the onset SIC of the peroxide crosslinked NR occurred. With further deformation, the crystal growth by oriented rubber chains in NRP was observed as shown in Fig. 4(a). In the case of filled rubber composites, filling CTBO and CTB particles (red or blue with green layers of bound rubber layers) into the composite material caused increased crosslinking points in the peroxide crosslinking system (as seen in Table 1), resulting in the decreased distance between the crosslinking points. The short chains in both filled NR composites were easily stretched and the onset SIC in the composite material was faster than that of NRP as seen in Fig. 4(b and c). The presence of organic components in CTBO particles slightly increased the bound rubber layer around the filler particles. However, the crystallinity index (Fig. 2(f)) and the crystallite size (L_{200}, L_{120}, L_{002}) as shown in Table 1 were comparable in both CTBO- and CTB-filled NR composites. The bound rubber affected the SIC of both filled NR composites in terms of the OAI value. It is interesting to note that the increase in the bound rubber layer around the cuttlebone particles by organic components could improve not only the compatibility between the inorganic filler and rubbery matrix but also the stress loading of the NR composite material (more stress loaded to immobilized phases), hence the lower OAI value in the case of NRCTBO (Fig. 3(b)). Accordingly, the role of organic components in cuttlebone particles on the reinforcement of NR composite material was clarified in this study.

Conclusions

The synergistic effects of cuttlebone particles with organic components on the morphological and mechanical properties of peroxide cross-linked cuttlebone/NR composites were investigated in this study. The AFM images confirmed that the organic components in cuttlebone particles improved the interfacial adhesions between the cuttlebone particles and the NR matrix. The results of simultaneous tensile/WAXD measurement revealed that the presence of the organic components in cuttlebone particles disturbed the NR chain orientation but did not prevent the SIC in peroxide cross-linked cuttlebone/NR composites. The relationship between the stresses and SIC parameters showed that the cuttlebone particles are the reinforcer that handles the stresses together with the oriented NR chains and the crystallites generated. Accordingly, this study indicated that the roles of organic components in cuttlebone particles are important for improving the high performance of rubber materials.

Author contributions

Thitipat Chongcharoenchaikul: data curation (lead); formal analysis (lead); investigation (equal); methodology (lead); visualization (equal); writing – original draft (lead). Kosuke Miyaji: data curation (supporting); investigation (supporting); methodology (supporting). Preeyanuch Junkong: formal analysis (supporting); investigation (supporting); methodology (supporting); validation (supporting); writing – review and editing (supporting). Sirilux Poompradub: conceptualization (lead); funding acquisition (lead); resources (lead); supervision (lead); validation (lead); writing – review and editing (lead). Yuko Ikeda: conceptualization (lead); funding acquisition (lead); resources (lead); supervision (lead); validation (lead); writing – review and editing (lead).

Conflicts of interest

The authors declare that they have no financial or other personal interests that could have appeared to influence the work reported in this paper.

Acknowledgements

This work was supported by the 100th Anniversary Chulalongkorn University Fund for Doctoral Scholarship, the 90th Anniversary of Chulalongkorn University Fund (Ratchadaphiseksomphot Endowment Fund) and the Overseas Research Experience Scholarship for Graduate Student. We acknowledge KIT Global Human Resource Development Program, 2018 Short-Term Student Exchange Program of Kyoto Institute of Technology for facilities support during the research. The WAXD experiment was performed in the BL-40XU at the SPring-8 with the approval of the Japan Synchrotron Radiation Research Institute (JASRI) (Proposal No. 2018B1274).

References

1 D. Roberts, *Natural Rubber Science and Technology*, Oxford University Press, Oxford, 1988.
2 L. Mullins, *The Chemistry and Physics of Rubber-Like Substances*, ed. L. Bateman, MacLaren & Sons, London, 1963, ch. 11, pp. 301–328.

3 E. H. Andrews and A. N. Gent, *The Chemistry and Physics of Rubber-Like Substances*, ed. L. Bateman, MacLaren & Sons, London, 1963, ch. 9, pp. 225–248.
4 *Chemistry, manufacture and applications of natural rubber*, ed. S. Kohjiya and Y. Ikeda, Elsevier, Woodhead Publishing, Oxford, 2014.
5 Y. Ikeda, A. Tohsan and S. Kohjiya, *Renewed Consideration on Natural Rubber Yielding Plants: A Sustainable Development Standpoint, Sustainable Development: Processes, Challenges and Prospects*, Nova Science Publishers, New York, 2015, ch. 3, pp. 65–85.
6 Y. Ikeda, A. Kato, S. Kohjiya and Y. Nakajima, *Rubber Science: A Modern Approach*, Springer, Singapore, 2017.
7 *Chemistry, Manufacture and Applications of Natural Rubber*, ed. S. Kohjiya and Y. Ikeda, Elsevier, Woodhead Publishing, Oxford, 2nd edn, 2021.
8 P. M. Visakh, S. Thomas, K. Oksman and A. P. Mathew, *Composites, Part A*, 2012, **43**, 735–741.
9 S. A. Bahari and A. Krause, *J. Cleaner Prod.*, 2016, **110**, 16–24.
10 H. W. Kwak, H. Lee, M. E. Lee and H. J. Jin, *J. Cleaner Prod.*, 2018, **200**, 1034–1042.
11 K. Zhang, F. Wang, W. Liang, Z. Wang, Z. Duan and B. Yang, *Polymers*, 2018, **10**, 608.
12 S. C. Chin, K. F. Tee, F. S. Tong, H. R. Ong and J. Gimbun, *Mater. Today Commun.*, 2020, **23**, 100876.
13 K. Aruchamy, S. P. Subramani, S. K. Palaniappan, B. Sethuraman and G. V. Kaliyannan, *J. Mater. Res. Technol.*, 2020, **9**, 718–726.
14 Y. Du, T. Wu, N. Yan, M. T. Kortschot and R. Farnood, *Composites, Part B*, 2018, **48**, 10–17.
15 Y. Igarashi, A. Sato, H. Okumura, F. Nakatsubo and H. Yano, *Chem. Eng. J.*, 2018, **354**, 563–568.
16 W. Lertwassana, T. Parnklang, P. Mora, C. Jubsilp and S. Rimdusit, *Composites, Part B*, 2019, **177**, 107280.
17 P. Pittayavinai, S. Thanawan and T. Amornsakchai, *Polym. Test.*, 2016, **54**, 84–89.
18 N. Hariwongsanupab, S. Thanawan, T. Amornsakchai, M. F. Vallat and K. Mougin, *Polym. Test.*, 2017, **57**, 94–100.
19 S. S. Todkar and S. A. Patil, *Composites, Part B*, 2019, **174**, 106927.
20 B. Surajarusarn, S. Hajjar-Garreau, G. Schrodj, K. Mougin and T. Amornsakchai, *Polym. Test.*, 2020, **82**, 106289.
21 S. Poompradub, Soft bio-composites from natural rubber (NR) and marine products, *Chemistry, Manufacture and Applications of Natural Rubber*, Woodhead Publishing, Cambrige, 2014, pp. 303–324.
22 S. Poompradub, Y. Ikeda, Y. Kokubo and T. Shiono, *Eur. Polym. J.*, 2008, **44**, 4157–4164.
23 P. Klungsuwan, A. Jarerat and S. Poompradub, *J. Polym. Environ.*, 2013, **21**, 766–779.
24 P. Kamalbabu and G. C. M. Kumar, *Procedia Mater. Sci.*, 2014, **5**, 802–808.
25 S. Shang, K. L. Chiu, M. C. W. Yuen and S. Jiang, *Compos. Sci. Technol.*, 2014, **93**, 17–22.
26 P. Kamalbabu and G. C. M. Kumar, *J. Compos. Mater.*, 2016, **50**, 807–823.
27 V. Fombuena, L. Bernardi, O. Fenollar, T. Boronat and R. Balart, *Mater. Des.*, 2014, **57**, 168–174.
28 A. J. Uddin, M. Fujie, S. Sembo and Y. Gotoh, *Carbohydr. Polym.*, 2012, **87**, 799–805.
29 V. Rubentheren, T. A. Ward, C. Y. Chee and C. K. Tang, *Carbohydr. Polym.*, 2015, **115**, 379–387.
30 J. Nie, W. Mou, J. Ding and Y. Chen, *Composites, Part B*, 2019, **172**, 152–160.
31 B. Ding, S. Huang, K. Shen, J. Hou, H. Gao, Y. Duan and J. Zhang, *Carbohydr. Polym.*, 2019, **225**, 115230.
32 J. Cadman, S. Zhou, Y. Chen and Q. Li, *J. Bionic Eng.*, 2012, **9**, 367–376.
33 T. Chongchareonchaikul, K. Miyaji, P. Junkong, S. Poompradub and Y. Ikeda, *J. Appl. Polym. Sci.*, 2022, e52375.
34 S. Kohjiya, A. Kato and Y. Ikeda, *Reinforcement of Rubber*, Springer, Singapore, 2020.
35 M. Tosaka, S. Murakami, S. Poompradub, S. Kohjiya, Y. Ikeda, S. Toki, I. Sics and B. S. Hsiao, *Macromolecules*, 2004, **37**, 3299–3309.
36 M. Tosaka, S. Kohjiya, S. Murakami, S. Poompradub, Y. Ikeda, S. Toki, I. Sics and B. S. Hsiao, *Rubber Chem. Technol.*, 2004, **77**, 711–723.
37 M. Tosaka, *Polym. J.*, 2007, **39**, 1207–1220.
38 Y. Ikeda, Y. Yasuda, S. Makino, S. Yamamoto, M. Tosaka, K. Senoo and S. Kohjiya, *Polymer*, 2007, **48**, 1171–1175.
39 A. Vieyres, R. Pérez-Aparicio, P. A. Albouy, O. Sanseau, K. Saalwächter, D. R. Long and P. Sotta, *Macromolecules*, 2013, **46**, 889–899.
40 P. A. Albouy, A. Vieyres, R. Pérez-Aparicio, O. Sanséau and P. Sotta, *Polymer*, 2014, **55**, 4022–4031.
41 S. Toki and B. S. Hsiao, *Macromolecules*, 2003, **36**, 5915–5917.
42 Y. Ikeda, N. Higashitani, K. Hijikata, Y. Kokubo, Y. Morita, M. Shibayama, N. Osaka, T. Suzuki, H. Endo and S. Kohjiya, *Macromolecules*, 2009, **42**, 2741–2748.
43 S. Toki, J. Che, L. Rong, B. S. Hsiao, S. Amnuaypornsri, A. Nimpaiboon and J. Sakdapipanich, *Macromolecules*, 2013, **46**, 5238–5248.
44 J. Che, C. Burger, S. Toki, L. Rong, B. S. Hsiao, S. Amnuaypornsri and J. Sakdapipanich, *Macromolecules*, 2013, **46**, 4520–4528.
45 Y. Ikeda, P. Junkong, T. Ohashi, T. Phakkeeree, Y. Sakaki, A. Tohsan, S. Kohjiya and K. Cornish, *RSC Adv.*, 2016, **6**, 95601–95610.
46 N. Candau, L. Chazeau, J. M. Chenal, C. Gauthier and E. Munch, *Phys. Chem. Chem. Phys.*, 2016, **18**, 3472–3481.
47 P. Junkong, K. Cornish and Y. Ikeda, *RSC Adv.*, 2017, **7**, 50739–50752.
48 P. V. L. Gac, P. A. Albouy and D. Petermann, *Polymer*, 2018, **142**, 209–217.
49 Y. Ikeda, Y. Yasuda, K. Hijikata, M. Tosaka and S. Kohjiya, *Macromolecules*, 2008, **41**, 5876–5884.
50 S. Poompradub, M. Tosaka, S. Kohjiya, Y. Ikeda, S. Toki, I. Sics and B. S. Hsiao, *J. Appl. Phys.*, 2005, **97**, 103529.
51 J. M. Chenal, C. Gauthier, L. Chazeau, L. Guy and Y. Bomal, *Polymer*, 2007, **48**, 6893–6901.

52 R. Pérez-Aparicio, A. Vieyres, P. A. Albouy, O. Sanséau, L. Vanel, D. R. Long and P. Sotta, *Macromolecules*, 2013, **46**, 8964–8972.
53 Y. Ikeda and A. Tohsan, *Colloid Polym. Sci.*, 2014, **292**, 567–577.
54 P. V. L. Gac, P. A. Albouy and P. Sotta, *Polymer*, 2019, **173**, 158–165.
55 Q. Demassieux, D. Berghezan, S. Cantournet, H. Proudhon and C. Creton, *J. Polym. Sci., Part B: Polym. Phys.*, 2019, **57**, 780–793.
56 T. Phakkeeree, Y. Ikeda, H. Yokohama, P. Phinyocheep, R. Kitano and A. Kato, *J. Fiber Sci. Technol.*, 2016, **72**, 160–165.
57 Y. Ikeda, T. Phakkeeree, P. Junkong, H. Yokohama, P. Phinyocheep, R. Kitano and A. Kato, *RSC Adv.*, 2017, **7**, 5222–5231.
58 A. Tunlert, P. Prasassarakich and S. Poompradub, *Mater. Chem. Phys.*, 2016, **173**, 78–88.
59 *SPring-8 web site*, **http://www.spring8.or.jp/en/**.